ELSEVIER

Computer Methods in Applied Mechanics and Engineering 129 (1996) 157–176

Computer methods in applied mechanics and engineering

An adaptive Petrov–Galerkin formulation for the compressible Euler and Navier–Stokes equations

Regina C. Almeida*, Augusto C. Galeão

Laboratório Nacional de Computação Científica, Rua Lauro Müller 455, 22290-160, Rio de Janeiro, Brazil

Received 12 October 1994

Abstract

In this paper we combine a stable Petrov–Galerkin formulation for the compressible Euler and Navier–Stokes equations with an *h*-adaptive remeshing refinement, including directional stretching and stretching ratio in the mesh regeneration procedure. The result is an accurate and efficient scheme appropriated to solve problems presenting shocks and boundary-layers.

1. Introduction

Among the difficulties associated with numerical simulation of compressible flows is the representation of shocks and boundary-layers. In those regions of the fluid flow, the variables in the system vary strongly, making the computation very challenging. In that case, it is well known that the approximate solution obtained by using the standard Galerkin finite element is completely spoiled by spurious oscillations that are spread all over the computational domain. In order to overcome or, at least, to minimize those oscillations many methods have been designed and we should mention the Petrov–Galerkin models which modify the Galerkin's weighting functions by adding a perturbation term but keeping the consistency property in the sense that the exact solution satisfies the approximate problem. Moreover, the possibility of using discontinuous weighting functions as first proposed in [1] with the SUPG (Streamline Upwind Petrov–Galerkin Method) opened a fascinating way to control those instabilities. The perturbation term in this method acts only in the streamline direction, chosen as the upwind direction, resulting in good stability and accuracy properties if the exact solution is regular, showing a convergence improvement over the Galerkin method. However, for non-regular solutions, those properties only worth out of a neighborhood containing sharp gradients, where spurious oscillations remain.

Considerable success has been achieved using the concept of approximate upwind direction, introduced by the CAU Method (Consistent Approximate Upwind Method) [2]. This idea yields a method that keeps the perturbation term over the streamline direction and adds, in a consistent way, a non-linear perturbation which provides the control over the derivatives in the direction of the approximate gradient, avoiding completely spurious oscillations. This method was originally designed for the convection-dominated convective-diffusive problems and its generalization was first presented in [3]. In this paper we cover with more details the generalization procedure and we combine the method with an *h*-adaptive remeshing refinement procedure. This was done because, in spite of the method, the finite element mesh near discontinuities in the flow must be fine

* Corresponding author.

SSDI 0045-7825(95)00858-6

enough in order to accurately solve all flow details. If the singularity position changes in time and/or three dimensional problems are considered, regular meshes lead to prohibit computational costs and core memory. Clearly, the use of an adaptive mesh refinement should be introduced into the existing finite element code as a standard feature and its efficiency will depend upon the quantitative error control to determine where the coarse grid accuracy is insufficient and locally create finer grid in these regions.

The development of a computable and reliable error estimator for the compressible Euler and Navier–Stokes equations is far from being an easy task, mainly because of the unsymmetrical operator, the nonlinearity and the amount of unknown physical variables (density, velocity, internal energy) appearing in such problems. The properties of these operators (hyperbolic for Euler problems and incompletely parabolic for Navier–Stokes flows) have to be taken into account for the design of an appropriate error estimator.

There has already been a variety of literature on adaptive methods in computational fluid dynamics. Many choose a key variable to guide the refinement process [4,5], loosing some information about the overall behavior of the fluid flow. In [6] an error indicator based on the residual of the governing equations is proposed.

In this paper we generalized the error indicator initially derived for scalar advection-diffusion problems in [7] based on the same norm used in [8] to prove stability and convergence rates for the SUPG method. Its efficiency lies on generating finer grids near sharp layers and coarse meshes for regions of smooth solutions, yielding a minimum required number of elements to reach a given prescribed error. We will show that an error indicator based on this norm works very well, even for nonlinear systems. An h-adaptive remeshing refinement strategy for unstructured meshes is used, including direction of stretching and stretching ratio, leading to a very effective adaptive scheme for steady-state solutions considered here. Other adaptive schemes for transient solution of compressible flows will be treated in a future work.

An outline of this paper is as follows. In Section 2 the CAU method for systems employing entropy variables is presented. In Section 3 the proposed adaptive scheme and the used strategy are described. In Section 4 numerical experiments are conducted and the conclusions are drawn in Section 5.

2. The generalized CAU method

2.1. Background

In order to gain additional insight, which will be useful in the generalization of the CAU operator, let us first summarize previous results presented in [2,9] concerning the CAU approximate solution for the scalar advection-diffusion equation

$$\varphi_{,t} + u \cdot \nabla\varphi = \nabla \cdot K\nabla\varphi + f \quad \text{in } \Omega \times (0,T], \quad \Omega \subset \Re^d, \quad 1 \leqslant d \leqslant 3, \tag{1}$$

with the appropriate boundary and initial conditions and u is a given vector velocity field, K is a (small) diffusion coefficient and f is a given source term. Let $\mathcal{U}_h$ denote a finite element subspace. For each time $t \in (0,T]$, $\varphi^h \in \mathcal{U}_h$ is the CAU's approximation for (1) if it satisfies

$$\int_\Omega \left[\left(\varphi^h_{,t} + u \cdot \nabla\varphi^h - f\right)\widehat{\varphi}^h + K\nabla\varphi^h \cdot \nabla\widehat{\varphi}^h\right] \mathrm{d}\Omega + \sum_{e=1}^{N_e} \int_{\Omega_e} L^h \tau_1 u \cdot \nabla\widehat{\varphi}^h \,\mathrm{d}\Omega + \sum_{e=1}^{N_e} \int_{\Omega_e} \tau_2 \mathcal{C} \nabla\varphi^h \cdot \nabla\widehat{\varphi}^h \,\mathrm{d}\Omega = 0, \qquad \forall \widehat{\varphi}^h \in \mathcal{U}_h, \tag{2}$$

where N_e is the total number of elements and

$$L^h = \varphi^h_{,t} + u \cdot \nabla\varphi^h - \nabla \cdot K\nabla\varphi^h - f$$

is the residual and at the initial time

$$\int_\Omega \left(\varphi^h - \varphi_o\right)\widehat{\varphi}^h \,\mathrm{d}\Omega = 0,$$

where φ_o is the initial condition. In order to simplify the presentation, we have assumed homogeneous boundary conditions. The first integral appearing in (2) reproduces the classical Galerkin formulation whereas the integral

under the first summation index comes from the SUPG method. τ_1 and τ_2 are the upwind functions as defined in [2].

The tensor $\mathcal{C} = (u - v^h) \otimes (u - v^h)$ is known as CAU operator, a $(m \cdot d \times m \cdot d)$ matrix where m is the number of variables; $m = 1$ for the scalar case. It plays the role of a discontinuity-capturing operator which controls derivatives in the direction of $\nabla\varphi^h$. In its definition an auxiliary vector field v^h is introduced, which is designed such that, in each element Ω_e, $e = 1, \ldots, N_e$,

$$|u - v^h|^2 = (u - v^h)^t (u - v^h) \leqslant |u - w^h|^2, \quad \forall w^h \in Q_h, \tag{3}$$

where

$$Q_h = \left\{ w^h;\ \varphi^h_{,t} + w^h \cdot \nabla\varphi^h - \nabla \cdot K\nabla\varphi^h - f = 0 \text{ in each } \Omega_e \right\}. \tag{4}$$

This condition ensures that $\varphi^h \xrightarrow[h\to 0]{} \varphi \implies v^h \xrightarrow[h\to 0]{} u$ and leads to

$$\begin{cases} u - v^h = \dfrac{L^h}{|\nabla\varphi^h|^2}\nabla\varphi^h & \text{if } |\nabla\varphi^h| \neq 0 \\ u - v^h = 0 & \text{if } |\nabla\varphi^h| = 0 \end{cases} \tag{5}$$

Moreover, from (1) and (4) we obtain the following restriction

$$(u - v^h) \cdot \nabla\varphi^h = L^h \tag{6}$$

which shows that the CAU term appearing in (2) can also be written as

$$\sum_{e=1}^{N_e} \int_{\Omega_e} \nabla\varphi^{h^t} (u - v^h)\, \tau_2 (u - v^h) \cdot \nabla\bar{\varphi}^h \, d\Omega. \tag{7}$$

REMARKS

(1) the formulation (2) is consistent in the sense that it is satisfied for $\varphi^h = \varphi$ since $L^h = 0$;

(2) the CAU operator introduces a non-linearity, since $(u - v^h)$ depends upon φ^h;

(3) $\mathcal{C}$ acts in the $\nabla\varphi^h$ direction, which means that it has components only in the base $\left(\frac{\nabla\varphi^h}{|\nabla\varphi^h|} \otimes \frac{\nabla\varphi^h}{|\nabla\varphi^h|}\right)$;

(4) $\mathcal{C}$ can also be obtained from the following eigenvalue problem:

$$\mathcal{C}\Phi = \lambda^2\Phi;\ \Phi^t\Phi = 1 \quad \text{with} \quad \Phi = \frac{\nabla\varphi^h}{|\nabla\varphi^h|}, \tag{8}$$

and the eigenvalue $\lambda \in \Re$ is obtained from

$$|u - v^h|^2 = (u - v^h)^t (u - v^h)\, 1 = \lambda^2 1, \tag{9}$$

$$(u - v^h)\, 1 = \lambda \frac{\nabla\varphi^h}{|\nabla\varphi^h|} \quad \text{and} \quad (u - v^h) \cdot \nabla\varphi^h = L^h \tag{10}$$

leading to

$$\begin{cases} \lambda = \dfrac{L^h}{|\nabla\varphi^h|} & \text{if } |\nabla\varphi^h| \neq 0 \\ \lambda = 0 & \text{if } |\nabla\varphi^h| = 0 \end{cases}$$

These problems reproduce the same results previously presented and are, as we will see in the following, more suitable for the generalization for multidimensional systems.

2.2. *The generalization*

We consider the symmetric form of the compressible Euler and Navier–Stokes equations by writing them in terms of the (physical) entropy variables [10]. The usage of these variables may be explained by the fact that the Galerkin formulation of the compressible Navier–Stokes equations based on the conservative variables lacks certain properties which are needed to establish stability proofs and convergence analyses [11,12].

Using the V-entropy variables, the compressible Navier–Stokes equations can be written in the following symmetric form:

$$A_0 V_{,t} + \widetilde{A} \cdot \nabla V = \nabla \cdot \widetilde{K} \nabla V + \wp \tag{11}$$

where $A_0 = \frac{\partial U}{\partial V}$ is symmetric and positive-definite; $\widetilde{A}_i = A_i A_0$ are symmetric; $\widetilde{K}$ is symmetric and positive semi-definite with $\widetilde{K}_{ij} = K_{ij} A_0$; $U = (U_j)_{j=1}^{m}$ is the conservation variables vector, $U^t = [\rho, \rho u_1, \ldots, \rho u_d, \rho e]$; ρ is the density; u_i is the velocity in ith direction, $i = 1, \ldots, d$; e is the total energy density, $\nabla^t(\cdot) = \left(I_m \frac{\partial(\cdot)}{\partial x_1}, \ldots, I_m \frac{\partial(\cdot)}{\partial x_d}\right)$; I_m is the identity matrix; $A_i = \frac{\partial F_i}{\partial U}$ is the Jacobian matrix where F_i is the Euler flux defined as:

$$F_i = \{u_i \rho, u_i \rho u_1 + p\delta_{1i}, \ldots, u_i \rho u_d + p\delta_{di}, u_i \rho e + p u_i\},$$

where p is the thermodynamic pressure and δ_{ij} is the Kronecker delta. The matrix K can be decomposed in two parts: $K = K^{\nu} + K^{h}$, where $F_i^{\nu} = K_{ij}^{\nu} U_{,j}$ and $F_i^{h} = K_{ij}^{h} U_{,j}$, $i, j = 1, \ldots, d$, are the viscous and heat fluxes, respectively, given by

$$F_i^{\nu^t} = \{0, \tau_{1i}, \ldots, \tau_{di}, \tau_{ik} u_i\}$$

and

$$F_i^{h^t} = \{0, 0, \ldots, 0, -q_i\}.$$

In those definitions, τ_{ij} is the viscous stress and q is the heat flux. Finally, $\wp$ is the source vector. In the following we consider the compressible Euler equations as a particular case of the Navier–Stokes equations when F_i^{ν} and F_i^{h} vanish and there is no source term.

We consider now the approximated solution residual

$$\mathcal{L}^h = A_0 V_{,t}^h + \widetilde{A} \cdot \nabla V^h - \nabla \cdot \widetilde{K} \nabla V^h - \wp \tag{12}$$

and we shall define a $(m \cdot d \times m)$ matrix, denoted by $\widetilde{\theta}^h$, such that

$$A_0 V_{,t}^h + \widetilde{\theta}^h \cdot \nabla V^h - \nabla \cdot \widetilde{K} \nabla V^h - \wp = 0. \tag{13}$$

Combining these two above equations yields

$$\left(\widetilde{A} - \widetilde{\theta}^h\right) \cdot \nabla V^h = \mathcal{L}^h. \tag{14}$$

In order to design the CAU operator for multidimensional systems let us first notice that the matrix A_0 ($A_0 : U \to V$) plays the role of a metric tensor on $\Re^m$. However, it is possible to rewrite (11) using I_m as a metric tensor, since A_0 is a positive-definite matrix, by changing the variables: $V = A_0^{-1/2} \chi$, $\widetilde{A}_i = A_0^{1/2} \widehat{A}_i A_0^{1/2}$, $\widetilde{K}_{ij} = A_0^{1/2} \widehat{K}_{ij} A_0^{1/2}$ and $\wp = A_0^{1/2} \widehat{\wp}$. In this case, the system (11) is written in the form:

$$\chi_{,t} + \widehat{A} \cdot \nabla \chi = \nabla \cdot \widehat{K} \nabla V + \widehat{\wp}. \tag{15}$$

To this form we can use the same idea presented for the scalar case: the operator C must have components only in the base $\left(\frac{\nabla \chi^h}{|\nabla \chi^h|} \otimes \frac{\nabla \chi^h}{|\nabla \chi^h|}\right)$. Recovering the original variables, using the inverse transformation $\chi = A_0^{1/2} V$, we have that such a base should be $\left([A_0^{1/2}] \nabla V^h \,/\, |\nabla V^h|_{A_0} \otimes [A_0^{1/2}] \nabla V^h \,/\, |\nabla V^h|_{A_0}\right)$, where $|\nabla V^h|_{A_0} = \left(\nabla V^{h^t} [A_0] \nabla V^h\right)^{1/2}$ denotes the modulus of ∇V^h with respect to a $(m \cdot d \times m \cdot d)$ matrix $[A_0] = \operatorname{diag}[A_0, \ldots, A_0]$. Then, it is quite clear that the operator C,

$$C = \left(\widetilde{A} - \widetilde{\theta}^h\right) \otimes \left(\widetilde{A} - \widetilde{\theta}^h\right) A_0^{-1} = \left(\widetilde{A} - \widetilde{\theta}^h\right) A_0^{-1} \left(\widetilde{A} - \widetilde{\theta}^h\right)^t, \tag{16}$$

must satisfy the generalized eigenvalue problem

$$C \mathcal{V} = \lambda^2 [A_0] \mathcal{V}; \quad \mathcal{V}^t [A_0] \mathcal{V} = 1 \quad \mathcal{V} = \frac{\nabla V^h}{|\nabla V^h|_{A_0}}, \tag{17}$$

where orthonormal condition must be done with respect to $[A_0]$. The eigenvalue $\lambda \in \Re^+$ and the matrix $(\tilde{A} - \tilde{\theta}^h)$ are uniquely defined combining (16) and (17) with:

$$\left[\left(\tilde{A} - \tilde{\theta}^h\right)^t [A_0^{-1}] \left(\tilde{A} - \tilde{\theta}^h\right)\right] \mathcal{U} = \lambda^2 A_0 \mathcal{U}; \quad \mathcal{U}^t A_0 \mathcal{U} = 1$$

$$\left(\tilde{A} - \tilde{\theta}^h\right) \mathcal{U} = \lambda [A_0] \mathcal{V} \quad \text{and} \quad \left(\tilde{A} - \tilde{\theta}^h\right) \cdot \nabla V^h = \mathcal{L}^h. \tag{18}$$

Solving these problems one has

$$\lambda^2 = \frac{|\mathcal{L}^h|^2_{A_0^{-1}}}{|\nabla V^h|^2_{A_0}}; \quad \mathcal{U} = \frac{A_0^{-1}\mathcal{L}^h}{|\mathcal{L}^h|_{A_0^{-1}}} \quad \text{and} \quad \left(\tilde{A} - \tilde{\theta}^h\right)^t = \frac{\mathcal{L}^h \left([A_0] \nabla V^h\right)^t}{|\nabla V^h|^2_{A_0}} \quad \text{if} \quad |\nabla V^h|_{A_0} \neq 0 \tag{19}$$

and $\mathcal{C}$ is given by

$$\mathcal{C} = \frac{[A_0] \nabla V^h \mathcal{L}^{h^t} A_0^{-1} \mathcal{L}^h \left([A_0] \nabla V^h\right)^t}{|\nabla V^h|^4_{A_0}} \quad \text{if} \quad |\nabla V^h|_{A_0} \neq 0. \tag{20}$$

REMARKS

(1) $|\tilde{A} - \tilde{\theta}^h|_{A_0^{-1}} = \left[\left(\tilde{A} - \tilde{\theta}^h\right)^t [A_0^{-1}] \left(\tilde{A} - \tilde{\theta}^h\right)\right]^{1/2} = \frac{(\mathcal{L}^h \mathcal{L}^{h^t})^{1/2}}{|\nabla V^h|_{A_0}}$, a $(m \times m)$ matrix, can be seen as the generalized modulus of the rectangular matrix $(\tilde{A} - \tilde{\theta}^h)$ and represents the counterpart of the modulus in the Euclidean metric of the $(d \times 1)$ vector $(u - v^h)$ appearing in the scalar case;

(2) $\tilde{\theta}^h$ is the unique element satisfying (13) such that $V^h \xrightarrow[h \to 0]{} V \iff \tilde{\theta}^h \xrightarrow[h \to 0]{} \tilde{A}$, or in other words

$$\lim_{h \to 0} \left|\tilde{A} - \tilde{\theta}^h\right|_{A_0^{-1}} \longrightarrow \text{Null matrix}_{m \times m}.$$

2.3. Variational formulation

We may now formulate the CAU method for (11) by using the time-discontinuous Galerkin method as the basis of our formulation. To this end, consider partitions $0 = t_0 < t_1 < \cdots < t_n < t_{n+1} < \cdots$ of $\Re^+$ and denote by $I_n = (t_n, t_{n+1})$ the nth time interval. The space-time integration domain is the 'slab' $S_n = \Re^d \times I_n$ with boundary $\Gamma = \Gamma \times I_n$ and denote by S_n^e the eth element in S_n, $e = 1, \ldots, (N_e)_n$, where $(N_e)_n$ is the total number of elements in S_n. For $n = 0, 1, 2, \ldots$ the space-time finite element space $\mathcal{U}_n^h$ consists of continuous piecewise polynomials on the slab S_n and may be discontinuous in time across the time levels t_n. The variational formulation consists of: Find $V^h \in \mathcal{S}_n^h$ such that for $n = 0, 1, 2, \ldots$

$$\int_{S_n} \hat{V}^h \cdot \mathcal{L}^h \, \mathrm{d}x \, \mathrm{d}t + \sum_{e=1}^{(N_e)_n} \int_{S_n^e} (A_0 \hat{V}^h + \tilde{A} \cdot \nabla \hat{V}^h) \cdot \tau^e \mathcal{L}^h \, \mathrm{d}x \, \mathrm{d}t +$$

$$\sum_{e=1}^{(N_e)_n} \int_{S_n^e} \nabla \hat{V}^h \cdot [A_0] \nabla V^h \left(\frac{\mathcal{L}^{h^t}}{|\nabla V^h|^2_{A_0}} \tau_c^e \mathcal{L}^h\right) \mathrm{d}x \, \mathrm{d}t +$$

$$\int_{\Re^d} \hat{V}^h(t_n^+) \cdot A_0 \left(V^h(t_n^+) - V^h(t_n^-)\right) \mathrm{d}x = 0, \qquad \forall \hat{V}^h \in \mathcal{U}_n^h, \tag{21}$$

where the last term represents the jump condition by which the information is propagated from one slab to the next. The term involving τ^e—the $(m \times m)$ matrix of intrinsic time scale as defined in [11]—is the SUPG contribution. Notice that the SUPG operator here is acting over the generalized characteristics. Such approach seems to be more appropriate when using the space-time formulation adopted in this work and provides more stability to the weak form in transient problems [13]. The discontinuity-capturing operator introduced by CAU corresponds to the third term in (21), where (19) was used. $\tau_c^e = \frac{h^e}{2} |\tilde{A} - \tilde{\theta}^h|^{-1}_{A_0^{-1}} = \frac{h^e}{2} \mathcal{U} \lambda^{-1} \mathcal{U}^t$ for the hyperbolic case and if a uniform mesh consisting of d-cube elements is used, where h^e is the characteristic length and λ and $\mathcal{U}$ are determined using (19). Otherwise

$$\tau_c^e = \mathcal{U} \zeta(\mathrm{Pe}) \mu_c^{-1} \mathcal{U}^t,$$

with

$$\begin{cases} \mu_c^2 = \lambda^2 \dfrac{|\nabla_\xi V^h|^2_{A_0}}{|\nabla V^h|^2_{A_0}} = \dfrac{|\mathcal{L}^h|^2_{A_0^{-1}}}{|\nabla V^h|^2_{A_0}} \dfrac{|\nabla_\xi V^h|^2_{A_0}}{|\nabla V^h|^2_{A_0}} & \text{if } |\nabla V^h|_{A_0} \neq 0 \\ \mu_c = 0 & \text{if } |\nabla V^h|_{A_0} = 0 , \end{cases}$$

where $(\nabla_\xi V^h)^t = \left[V^h_{,1} \frac{\partial \xi_1}{\partial x_i}, \ldots, V^h_{,1} \frac{\partial \xi_d}{\partial x_i}\right]$, Pe is the Peclet number (see [14]) and $\zeta(\mathrm{Pe}) = \coth \mathrm{Pe} - 1/\mathrm{Pe}$ for linear elements. Using these results in (21), the CAU term is written as

$$T_{\mathrm{CAU}} = \sum_{e=1}^{(N_e)_n} \int_{S_n^e} \zeta(\mathrm{Pe}) \mu_c^{-1} \frac{|\mathcal{L}^h|^2_{A_0^{-1}}}{|\nabla V^h|^2_{A_0}} \nabla \hat{V}^{h^t} [A_0] \nabla V^h \, \mathrm{d}x \, \mathrm{d}t. \tag{22}$$

In order to avoid the double effect when the approximate gradient direction coincides with the generalized SUPG direction, we should subtract the projection of the SUPG operator in this direction (see [15] and [16]). Let us call η_e the function to be designed to compensate this effect. Thus, defining $\overline{A}^t = [A_0, \widetilde{A}_1, \ldots, \widetilde{A}_d]$ and $\overline{\nabla}^t(\cdot) = \left[I_m \frac{\partial(\cdot)}{\partial t}, I_m \frac{\partial(\cdot)}{\partial x_1}, \ldots, I_m \frac{\partial(\cdot)}{\partial x_d}\right]$ and using (21) we have

$$\nabla V^{h^t} \left(\widetilde{A} - \widetilde{\theta}^h\right) \mathcal{U} \eta_e \mathcal{U}^t \left(\widetilde{A} - \widetilde{\theta}^h\right)^t \nabla V^h = \overline{\nabla} V^{h^t} \overline{A} \tau^e \mathcal{L}^h.$$

Using now (14) and (19), η_e is determined as

$$\eta_e = \frac{\overline{\nabla} V^{h^t} \overline{A} \tau^e \mathcal{L}^h}{|\mathcal{L}^h|^2_{A_0^{-1}}} \tag{23}$$

and τ_c^e can be redefined as

$$\tau_c^e = \max \left\{ 0, \ \mathcal{U} \zeta(\mathrm{Pe}) \mu_c^{-1} \mathcal{U}^t - \mathcal{U} \frac{\overline{\nabla} V^{h^t} \overline{A} \tau^e \mathcal{L}^h}{|\mathcal{L}^h|^2_{A_0^{-1}}} \mathcal{U}^t \right\}. \tag{24}$$

The resulting CAU term can be written now as

$$T_{\mathrm{CAU}} = \sum_{e=1}^{(N_e)_n} \int_{S_n^e} \max \left\{ 0, \ \zeta(\mathrm{Pe}) \mu_c^{-1} \frac{|\mathcal{L}^h|^2_{A_0^{-1}}}{|\nabla V^h|^2_{A_0}} - \frac{\overline{\nabla} V^{h^t} \overline{A} \tau^e \mathcal{L}^h}{|\nabla V^h|^2_{A_0}} \right\} \nabla \hat{V}^{h^t} [A_0] \nabla V^h \, \mathrm{d}x \, \mathrm{d}t. \tag{25}$$

3. The adaptive refinement method

3.1. Preliminaries

In this work we will only apply the adaptive scheme in the search of the steady state solution of the bidimensional compressible Euler and Navier–Stokes equations. In such nonlinear problems it is known that a good strategy is to get the steady state solution from the limit solution of a time-dependent problem. Thus, the adaptive remeshing scheme combined with the CAU method consists in performing the calculations beginning with an initial coarse mesh until the steady state is reached; then, the error is estimated and, if the prescribed accuracy has not been satisfied, a new mesh is generated and the calculations are carried out using as initial condition the values of the variables interpolated at the nodes on the new mesh. Each new mesh is generated using the ARANHA code [17] by specifying at the nodes of the old mesh: (i) the new element length h_i^{new}; (ii) the stretching direction θ_i and (iii) the stretching ratio S_i. The main difficulty lies in how to determine each h_i^{new}. As we will show in the following, h_i^{new} is obtained by the proposed error indicator. θ_i is taken normal to the direction of the maximum change of density (the direction of the approximated density gradient). S_i is determined according to the methodology proposed in [5] by which S_i should be larger in regions where the flow is nearly one-dimensional. In order to avoid meshes too distorted, the stretching ratio may vary between $S_{i_{\min}}$ and $S_{i_{\max}}$.

3.2. A posteriori error indicator

The error may be measured with a variety of norms and such a choice often determines the efficiency of the whole adaptive scheme. Regarding to the ability to predict singularities in the fluid flow, the error indicator proposed in [7] stands out from others by its high accuracy and low computational effort using h-mesh refinement. Derived in order to obtain steady-state solution for scalar advection-diffusion problems, it was designed based on the norm applied in [8] to lead to optimal and near optimal error estimates for the SUPG method. Using this error indicator, in [18] better results were obtained using mesh regeneration taking into account stretching and mesh orientation according to the streamlines.

The convergence analysis of the generalized SUPG formulation for linear time-dependent multidimensional advective-diffusive systems were performed in [13] yielding uniform error estimates analogous to the scalar case. Indeed, the norm used in this case has the same features of its scalar counterpart. Then, it seems quite natural to design our error indicator in this way, even for the nonlinear compressible Euler and Navier–Stokes equations. Thus, for each element e, $e = 1, \ldots, (N_e)_n$, the error indicator to be used in this paper is defined as:

$$\epsilon_e^2 = \int_{\Omega_e} \nabla^* \boldsymbol{\epsilon} \cdot \tilde{K} \nabla^* \boldsymbol{\epsilon} \, d\Omega + \int_{\Omega_e} \left(\tilde{A} \cdot \nabla^* \boldsymbol{\epsilon} \right) \cdot \tau \left(\tilde{A} \cdot \nabla^* \boldsymbol{\epsilon} \right) d\Omega \tag{26}$$

where $\nabla^* \boldsymbol{\epsilon} = \nabla^* V - \nabla V^h$. Here, $\nabla^* V \in \left[C^0(\Omega) \right]^m$ is an approximation of the exact gradient solution, obtained by nodal averaging of the discontinuous ∇V^h surrounding each node. The square of the global $\boldsymbol{\epsilon}$ can be determined by summing all element contributions:

$$\boldsymbol{\epsilon} = \left[\sum_{e=1}^{(N_e)_n} \epsilon_e^2 \right]^{1/2} \tag{27}$$

3.3. The adaptive strategy

We adopt here the adaptive strategy presented in [19] which seeks an optimal mesh in the sense that the error is equally distributed for all elements. We will denote such a desired error by

$$\bar{\boldsymbol{\epsilon}}_m = \bar{\eta} \left[\frac{\sum_{e=1}^{(N_e)_n} \left(\|V^h\|_e^2 + \epsilon_e^2 \right)}{N} \right]^{1/2} \tag{28}$$

where $\bar{\eta}$ is the specified maximum admissible percentage error. The term under the summation is an approximation for $\|V\|^2$ (V is the unknown exact solution) and $\|\cdot\|$ is determined applying the same definition used for the error indicator (26).

Once the ratio $\xi_e = \epsilon_e / \bar{\epsilon}_m$ has been computed, the new length is determined according to

$$\left.\begin{array}{ll} \xi_e > 1 & \xrightarrow{\text{refinement}} \\ \xi_e \leqslant 1 \quad \Rightarrow \quad \xi_e := \xi_e + \frac{(1-\xi_e)}{\text{dmp}} & \xrightarrow{\text{unrefinement}} \end{array}\right\} \quad h_e^{\text{new}} = \frac{h_e^{\text{old}}}{\xi_e}. \tag{29}$$

REMARKS

(1) the nodal values h_i^{new} for each node i is obtained carrying out the point average of all h_e^{new} surrounding the node i;

(2) dmp is introduced so that h_e^{new} will not grow too fast;

(3) the error estimate given in [8] for regular mesh, smooth solutions and linear interpolation yields $\|V - V^h\| \leqslant C h^{3/2}$. As we are interested in representing singularities, we reduce this rate ($\frac{3}{2} \to 1$). This amounts to specifying in each element

$$\epsilon_e \approx C h_e^{\text{old}} \quad \text{and} \quad \bar{\epsilon}_m \approx C h_e^{\text{new}}$$

leading to (29);

(4) the maximum (h_{max}) and minimum (h_{min}) admissible element length are specified during the remeshing process.

4. Numerical results

In this section we give some numerical results obtained by applying the proposed methodology on the solution of a variety of compressible Euler and Navier–Stokes flow problems. Since we shall compare our formulation with others, we will here refer to SUPG as the generalized SUPG method presented in [14] and DCQ as the Galerkin least-square method with a quadratic discontinuity-capturing method developed in [11]. In all examples we will consider compressible polytropic gases with adiabatic exponent $\gamma = c_p/c_v = 1.4$.

All computations were done using linear elements in space discretization, constant in time discretization for steady problems and linear in time for transient problems.

4.1. One-dimensional steady shock problem

We consider here two flow regions of an inviscid compressible gas separated by a shock. The initial conditions are $\rho = 1$, $p = 0.17857$ and $u_1 = 1$ for $0 \leqslant x < 19.5$ and $\rho = 2.66667$, $p = 0.80357$ and $u_1 = 0.375$ for $19.5 < x \leqslant 39.0$, where p is the thermodynamic pressure. Since these values satisfy the normal shock condition, a stationary shock is formed for $x = 19.5$. To avoid ambiguous initial conditions at this point we used a mesh with 39 square elements.

The computed densities are presented in Fig. 1 showing the shock position. The SUPG presents some oscillations in a vicinity of the shock which disappear by using CAU and DCQ (the DC solution coincides with CAU's for this problem). Moreover, the CAU is less diffusive, resulting in the sharpest shock.

4.2. Flow over a wedge

This problem deals with an inviscid supersonic flow (Mach number $M = 2$) over a wedge at an angle with respect to the mesh. It is illustrated in Fig. 2 where the dashed line shows the position of the shock determined analytically.

To solve this problem numerically we used a structured mesh of 20×20 elements on a unit square domain. At the inflow all variables are fixed as shown in Fig. 2 and the slip condition was set along the wedge. It is

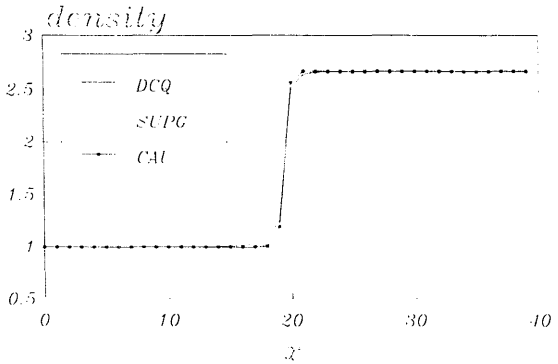

Fig. 1. Normal shock: computed densities.

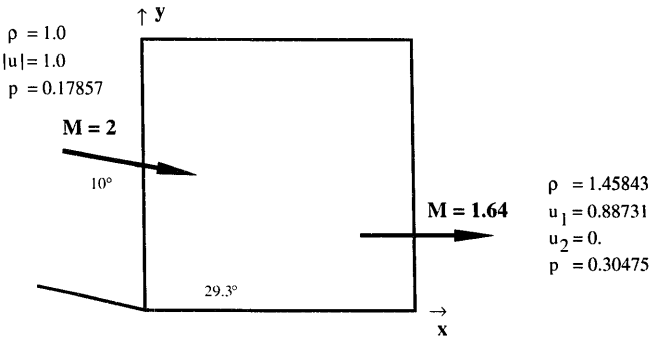

Fig. 2. Flow over a wedge: problem statement.

also shown in Fig. 2 the outflow exact solution which satisfies the Rankine–Hugóniot shock condition. The computed densities along $x = 0.9$ are depicted in Fig. 3. Both DCQ and CAU preclude oscillations and verify the R-H condition, but in this case CAU leads to a slightly more diffusive solution.

We also solved this problem incorporating the adaptive method. Notice that in this case $\tilde{A} \cdot \nabla V = 0$ and prescribing a percentage error does make any sense since $\|V\|^2 = \sum_{e=1}^{N} \int_{\Omega_e} (\tilde{A} \cdot \nabla V) \cdot \tau (\tilde{A} \cdot \nabla V)\, d\Omega = 0$. Thus, the refinement here will be guided specifying a maximum tolerance defined by $\text{tol} = \Theta \epsilon_{\max}$ where

$$\epsilon_{\max} = \max_{e=1,\ldots,N} (\epsilon_e) \quad \text{and} \quad \Theta < 1.$$

The algorithm halts when the relative difference between two consecutive steady state solutions is under a predefined tolerance.

Beginning with the mesh depicted in Fig. 4, we give in Fig. 5 the final mesh and level curves of density obtained using the proposed adaptive scheme. In Fig. 6, we present the correspondent results obtained using

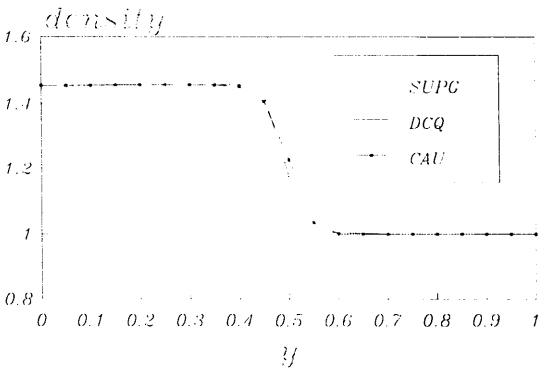

Fig. 3. Oblique shock: computed densities along $x = 0.9$.

the methodology proposed in [6] which leads to a refinement strategy: $Ch_i^{\text{new}}|\mathcal{L}^h| = \text{tol}$, tol being a predefined tolerance (we assume here $C = 1$). For both calculations we use dmp = 1.5, $S_{i_{\min}} = 1$ and $S_{i_{\max}} = 3$.

In Fig. 7 we compare the performance of these schemes and in Fig. 8 we present the final mesh obtained using a faster unrefinement (dmp = 2).

REMARKS

(1) the scheme proposed here and the one introduced in [6] are similar for this inviscid problem by the fact that $\mathcal{L}^h = \tilde{A} \cdot \nabla V^h$ and thus both depend upon $|\mathcal{L}^h|$. However, for our scheme a possible over-refinement is consistently and automatically prevented by the residual weighted L_2-norm, τ being the weighting function;

(2) the proposed scheme works very well for a faster unrefinement, keeping the accuracy and guiding the refinement at the correct place;

(3) during these calculations, the methodology used to determine the stretching ratio and stretching direction is proved to be very effective: if we adopted no stretching, the total number of nodes would grow more than two times.

4.3. Supersonic flow over a flat plate

This classical example, called Carter's problem, consists of a two-dimensional Mach 3 viscous flow over a semi-infinite flat plate at zero angle of attack. The problem statement and the boundary conditions are shown in Fig. 9. The subscript ∞ refers to the undisturbed flow: $\rho_\infty = 1$; $U_\infty = 1$ and $\theta_\infty = 2.769 \cdot 10^{-4}$. The stagnation temperature $\theta_{\text{stag}} = \theta_\infty \left(1 + \frac{1}{2}(\gamma - 1)M_\infty^2\right)$ is prescribed on the plate and the Sutherland's law is employed to model the dependence of viscosity on temperature.

The iso-pressure and Mach number obtained using CAU with a structured mesh of 56×32 elements are shown in Figs. 10 and 11. The computed densities along $x = 1.0$ using DCQ and CAU are shown in Fig. 12. The agreement between the two solutions is good except that they lead to different shock positions. If we compare these results with Carter's finite difference calculations [21], who validated his results by comparison with analytical curves based on a Blasius boundary layer approximation, we verify that CAU yields the best shock position.

The sequence of space mesh and level curves of density, temperature and pressure depicted in Figs. 13 and 14

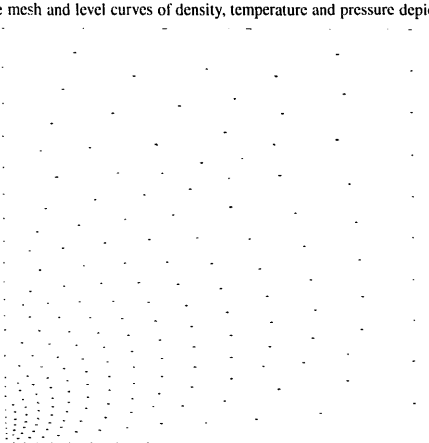

Fig. 4. First mesh (226 nodes/396 elements).

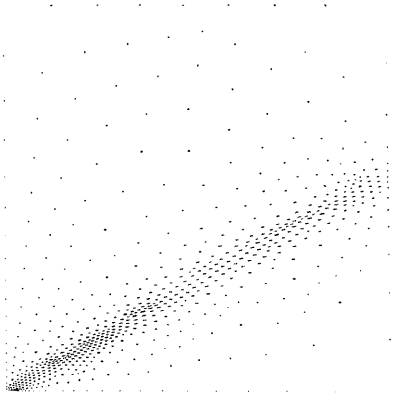

Fig. 5. Final mesh (682 nodes/1292 elements) and density solution.

shows the ability of the adaptive scheme in representing the overall behavior of this viscous fluid flow. These results were obtained using $\overline{\eta} = 15\%$.

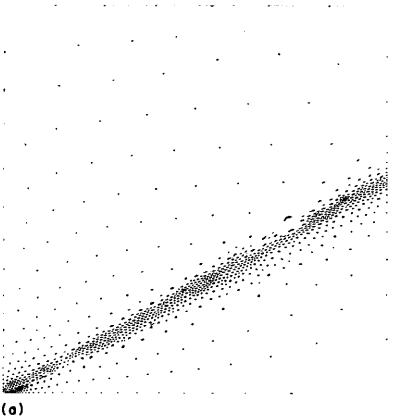

Fig. 6. Final mesh (1023 nodes/1967 elements) and density solution.

4.4. *Riemann shock tube problem*

This transient problem deals with two flow regions of an inviscid compressible gas in a uniform tube with a diaphragm at the mid section. The fluid properties for the fluid at rest are $\rho = p = 1$ on $0 \leqslant x \leqslant 0.5$ and $\rho = 0.125$, $p = 0.1$ on $0.5 < x \leqslant 1.0$. When the diaphragm is broken, a shock wave moves downstream and

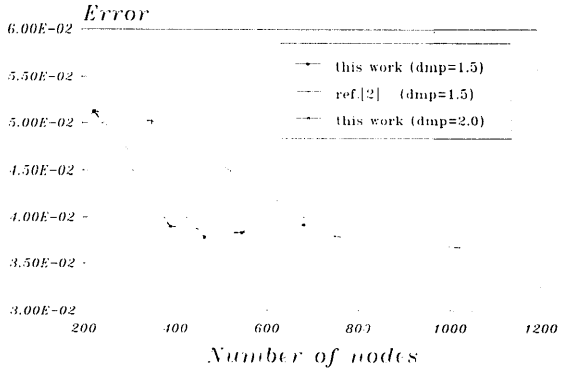

Fig. 7. Computed error measured by (21).

a rarefaction lies upstream of the initial position. The approximate solutions at $t = 0.14$ are shown in Fig. 15. In spite of being more diffusive, the CAU precludes the oscillations caused by an ineffective control of DCQ. Both results are obtained for the stable Courant number for each method and DCQ led to greater time steps (dt): the dt stable for CAU is about ten times smaller. However, the reduction of dt yields more oscillating solutions for DCQ (Fig. 16), what does not happen when shorter time steps are used with CAU method.

5. Conclusions

In this paper we have given a stable method for solving the compressible Euler and Navier–Stokes equations written in entropy variables, designed using a space-time finite element formulation. The numerical results showed that this model is very stable, providing accurate approximate solutions near shocks and boundary-layers free of spurious oscillations. The accuracy was improved by incorporating the developed adaptive remeshing scheme, as proposed in Section 3. The error indicator is able to identify precisely the shock and boundary-layer regions of the fluid flow, guiding the refinement to the correct place. The directional stretching and stretching ratio procedure yield a faster convergence numerical model.

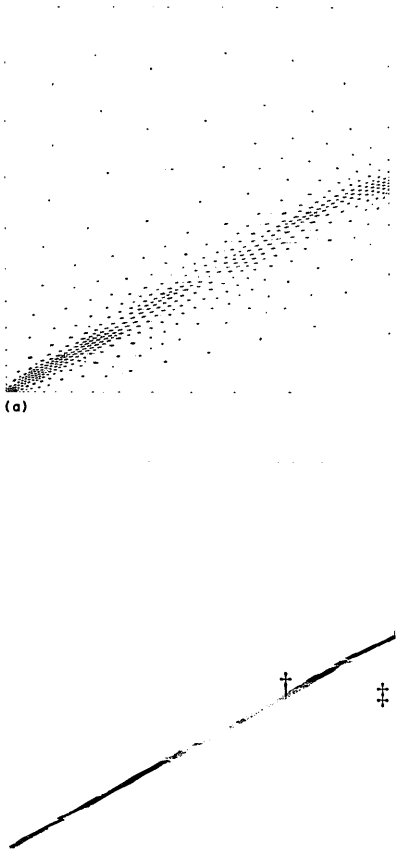

Fig. 8. Final mesh (547 nodes/1037 elements) and density solution dmp = 2.

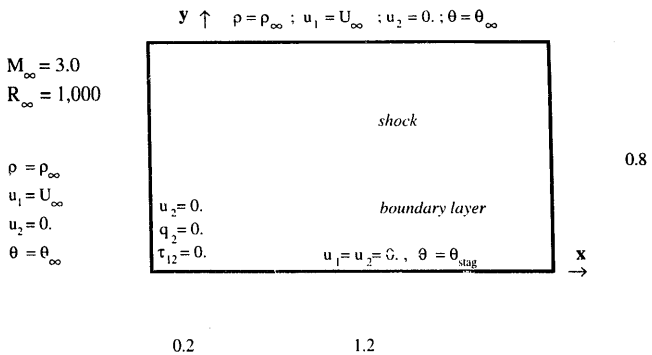

Fig. 9. Flat plate: problem statement.

Fig. 10. Flat plate: iso-lines of the computed pressure.

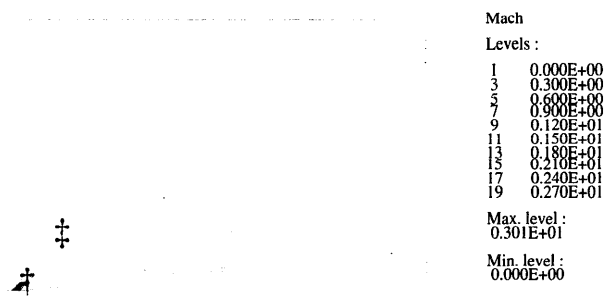

Fig. 11. Flat plate: iso-lines of the computed Mach number.

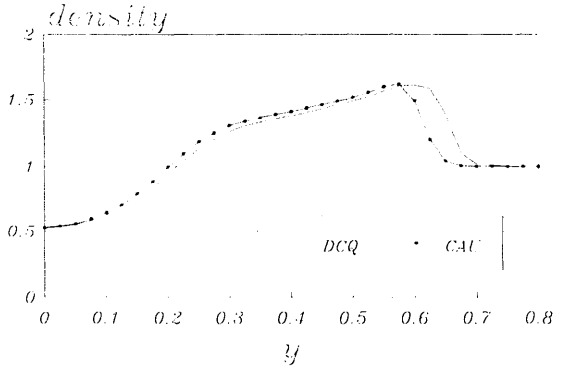

Fig. 12. Flat plate: computed densities along $x = 1.0$.

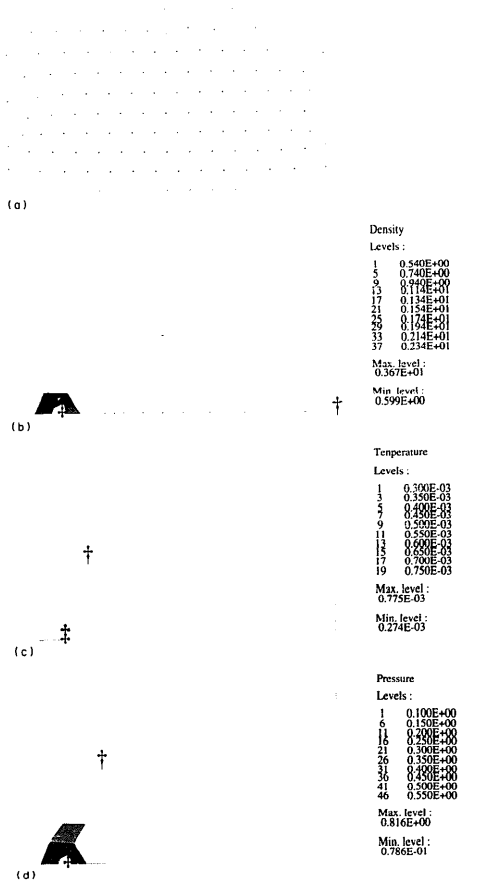

Fig. 13. First mesh (368 nodes/248 elements) and associated solution.

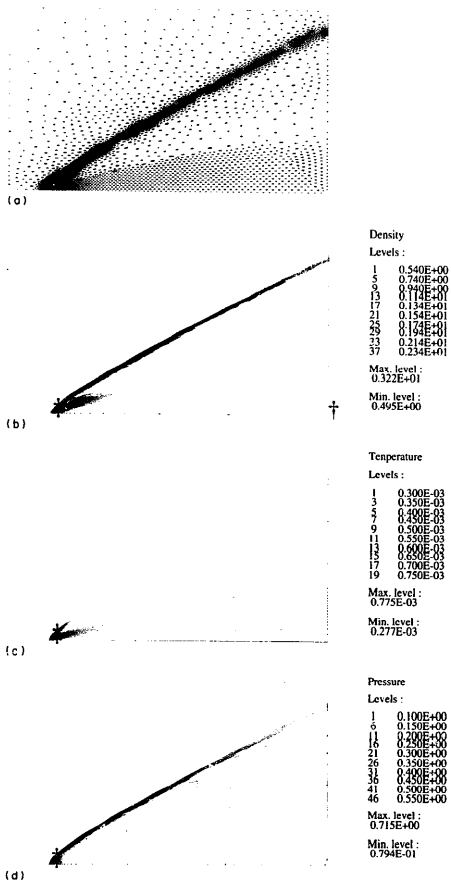

Fig. 14. Final mesh (3687 nodes/7206 elements) and associated solution.

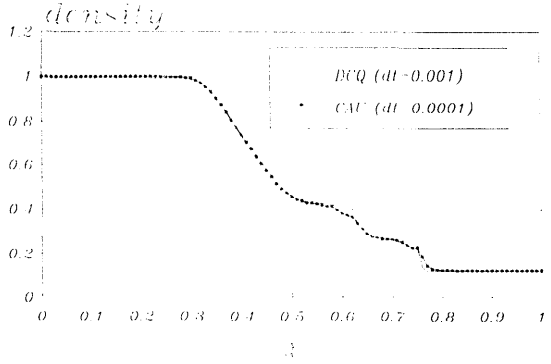

Fig. 15. Riemann shock tube: computed densities for $t = 0.14$.

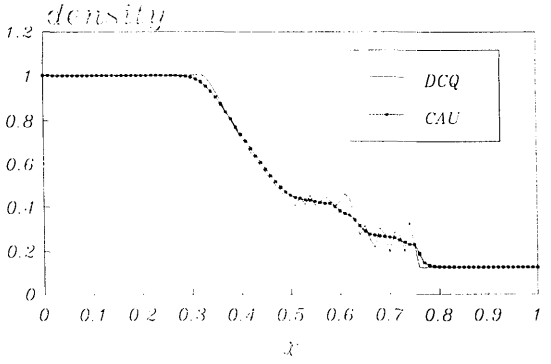

Fig. 16. Riemann shock tube: computed densities for $t = 0.14$ and $dt = 0.0001$.

References

[1] A.N. Brooks and T.J.R. Hughes, Streamline upwind Petrov–Galerkin formulations for convection-dominated flows with particular emphasis on the incompressible Navier–Stokes equations, Comput. Methods Appl. Mech. Engrg. 32 (1982) 199–259.

[2] A.C. Galeão and E.G. Do Carmo, A consistent approximate upwind Petrov–Galerkin method for convection-dominated problems, Comput. Methods Appl. Mech. Engrg. 68 (1988) 83–95.

[3] R.C. Almeida and A.C. Galeão, The generalized CAU operator for the compressible Euler and Navier–Stokes equations, 8th International Conference on Numerical Methods in Laminar and Turbulent Flows, 1993.

[4] J.T. Oden, L. Demkowicz, T. Strouboulis and P. Devloo, Adaptive methods for problems in solid and fluid mechanics, in: Accuracy Estimates and Adaptive Refinements in Finite Element Computations (Wiley, Lisboa, 1984).

[5] C.J. Hwang and S.J. Wu, Global and local remeshing algorithms for compressible flows, J. Comput. Phys. 102 (1992) 98–113.

[6] P. Hansbo and C. Johnson, Adaptive streamline diffusion methods for compressible flow using conservation variables, Comput. Methods Appl. Mech. Engrg. 87 (1991) 267–280.

[7] R.S. Silva and A.C. Galeão, A posteriori error estimator for Petrov–Galerkin models applied to problems with boundary-layers, 11th ABCM Mech. Engrg. Conf. (1991) 193–196 (in Portugese).

[8] C. Johnson, U. Nävert, and J. Pitkaranta, Finite element methods for linear hyperbolic problems, Comput. Methods Appl. Mech. Engrg. 45 (1984) 285–312.

[9] E.G. Do Carmo and A.C. Galeão, Feedback Petrov–Galerkin methods for convection-dominated problems, Comput. Methods Appl. Mech. Engrg. 88 (1991) 1–16.

[10] T.J.R. Hughes, L.P. Franca and M. Mallet, A new finite element formulation for computational fluid dynamics. Part I: Symmetric forms of the compressible Euler and Navier–Stokes equations and the Second Law of thermodynamics, Comput. Methods Appl. Mech. Engrg. 54 (1986) 223–234.

[11] F. Shakib, Finite element analysis of the compressible Euler and Navier–Stokes equations, Ph.D. Thesis, Stanford University, 1988.

[12] C. Johnson, A. Szepessy and P. Hansbo, On the convergence of shock-capturing streamline diffusion finite element methods for the hyperbolic conservation laws, Math. Comput. 54 (1990) 107–129.

[13] T.J.R. Hughes, L.P. Franca and M. Mallet, A new finite element formulation for computational fluid dynamics. Part VI: Convergence analysis of the generalized SUPG formulation for linear time-dependent multidimensional advective-diffusive systems, Comput. Methods Appl. Mech. Engrg. 63 (1987) 97–112.

[14] T.J.R. Hughes and M. Mallet, A new finite element formulation for computational fluid dynamics. Part III: The generalized streamline operator for multidimensional advective-diffusive systems, Comput. Methods Appl. Mech. Engrg. 58 (1986) 305–328.

[15] M. Mallet, A Finite Element Method for Computational Fluid Dynamics, Ph.D. Thesis, Stanford University, 1985.

[16] R. Almeida and R. Silva, A new Petrov–Galerkin method for convection-dominated problems, Comput. Methods Appl. Mech. Engrg., submitted for publication.

[17] E.A. Fancello, A.C.S. Guimarães, R.A. Feijóo and M. Venere, A 2D automatic mesh generator in oriented object language, 11th ABCM Mech. Engrg. Conf. (1991) 635–638 (in Portugese).

[18] R.S. Silva and A.C. Galeão, Adaptive formulations applied to advective-diffusive problems, 12th ABCM Mech. Engrg. Conf. 1993.

[19] O.C. Zienkiewicz and J.Z. Zhu, A simple error estimator and adaptive procedure for practical engineering analysis, Int. J. Numer. Methods Engrg. 24 (1987) 337–357.

[20] J.E. Carter, Numerical solutions of the Navier–Stokes equations for the supersonic laminar flow over a two-dimensional compression corner, NASA TR, R-385 (1972) 21–29.

[21] P. Devloo, J.T. Oden and P. Pattani, An h-p adaptive finite element method for the numerical simulation of compressible flow, Comput. Methods Appl. Mech. Engrg. 70 (1988) 203–235.